Blood flow analysis through complex microvessels by digital image velocimetry

Swaroop S. Singh and Megha Singh

Biomedical Engineering Division, Indian Institute of Technology, Chennai 600 036, India

The image velocimetry, based on the variation of the brightness in a sequence of images, is applied to analyse complex pulsatile blood flow through frog mesenteric arterial branching. The images of blood flow are obtained by videomicroscopic system. After determination of cardiac cycle, four segments are selected to determine the variation in flow pattern through analysis of axial velocity. During systolic phase the flow is in the forward direction in the main and branch arteries but reverses during the diastolic phase, leading to altered flow conditions in the main artery. Based on analysis by this technique, the changes in flow pattern at various locations in the arteries are determined.

Blood flow through arterial microvessels is of pulsatile nature and complex due to viscoelastic properties of blood vessels and their various configurations. In these the variability of flow velocity is the consequence of generation of secondary flow at complex geometries[1] which could be attributed primarily to the effect of the centrifugal pressure gradient in the main flow acting on a relatively stagnant fluid in the wall boundary layer[2]. Several techniques have been developed to measure blood flow in microvessels. Prominent among these are laser Doppler anemometry[3], high speed microcinephotography[4], two-slit photometry, dual-sensor microscopy[5], epifluorescence microscopy[6], etc.

Blood flow is the major contributor to metabolic exchange between tissues and blood. Although this mechanism takes place in capillaries, the pre-capillary vessels (of diameter less than 0.01 mm) play an important role in this process. Hence the flow pattern in these vessels resulting due to variation in geometries of the vessels, is an important contributor to flow through these vessels. But as such these vessels are not accessible for flow recording and its analysis.

With the advancement of medical diagnostic techniques such as angiography, axial tomography and magnetic resonance imaging it is now possible to record/reconstruct the images. For further improvement in diagnosis there is a need to measure the changes in flow pattern in clinical conditions from the sequence of such images. Recently, using digital flow visualization[7], we have developed a technique and applied it successfully to microscopic images to analyse blood flow in straight[8] and curved[9] glass capillaries. The erythrocyte distribution and velocity profiles are determined by axial tomographic[10] and image velocimetry[11] techniques, respectively. But the blood flow analysis in rigid glass tubes is not the exact simulation of that in the cardiovascular system[1] and such variation could easily be shown through our recent study on blood flow through frog mesenteric arterial branching under steady flow conditions[12].

During pulsatile flow conditions the pressure and flow in blood vessels vary over a cardiac (flow) cycle. The analysis carried out under steady flow conditions represents a single phase of the flow cycle. In contrast to straight vessels the situation may become further complex if flow through a branch of a curved artery is not unidirectional but reverses during the diastolic phase of the cardiac cycle. The analysis of such a flow condition forms the objective of the present study and has been carried out on the videomicroscopic images of the blood flow through frog curved mesenteric curved branching artery. As the erythrocyte distribution profiles match closely with that of velocity profiles in complex geometries, in the present study the variation in the velocity only over a cardiac cycle by image velocimetry is determined.

Figure 1 shows the schematic of the experimental set-up. Prior to data recording, to restrict the movement of the frog, the nervous centre was destroyed by pithing and the spinal cord was left intact to maintain blood flow and respiration. The abdomen was cut open and part of the mesentery containing microvessels was gently mounted on a small hole made in a thin thermocole sheet. The sheet was mounted on the stage of a microscope in such a way that the mesenteric vessel was aligned with the viewing axis of the microscopic system. By X–Y movement of the stage, the curved branching was located. The open area near the recording site was moistened with a gauze wet with physiological saline to prevent it from drying.

For recording the pulsatile blood flow through the arterial microvessel the microscope (Dialux22, Leitz, Germany) in transmission mode was used. A well collimated beam of light from a 12 V, 100 W tungsten halogen lamp was achieved by using a field diaphragm and by incorporating an interchangeable condenser, with the condenser top turned in (supplementary lens turned out), essentially required for the objective of aperture

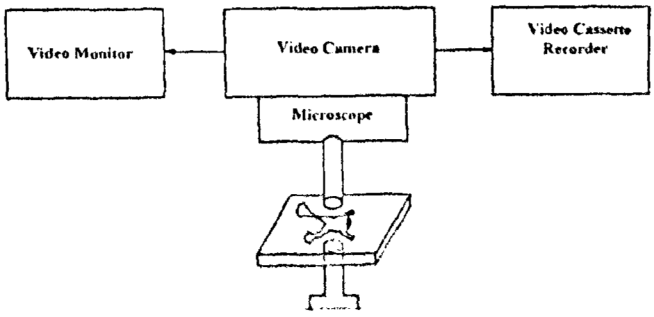

Figure 1. Schematic of the experimental set-up

larger than 0.25. The objective used in this study was NPL Fluotar of magnification 16×/0.45. For recording, the objective was focused on the diametric plane of the main artery. Thereafter this was carried out at the rate of 25 frames/second in a videotape using a VHS cassette recorder.

Figure 2 shows the schematic of the data analysis system to obtain the velocity distribution profiles from the sequentially recorded data by the procedure mentioned above. An IBM PC/AT compatible incorporated with Matrox MVP/AT/NP image processing card was used. The video memory of the system was $4 \times 512 \times 512$ or $64 \times 128 \times 128$ grey levels. For sequential analysis of blood flow images, 64 successive frames after digitization could be stored in the computer. Further details of this system are given elsewhere[8,9].

The relative motion between the objects in a field and a camera gives rise to apparent motion of objects in a sequence of images[11,13]. Optical flow is the distribution of the apparent velocities of movement of brightness pattern in an image. To measure the two-dimensional velocity in arterial branching, two successive frames of 128×128 pixels resolution and 256 grey levels were analysed. Prior to implementation of optic flow algorithm, the following operations required to pre-process the image were carried out:

(a) *Edge detection*: As the edges in the image indicate a sudden transition in the grey level intensity, they are enhanced by Sobel edge operator[14].

(b) *Thresholding*: In this operation the pixel grey levels are compared with a selected threshold value and are classified depending on whether the grey level is above this value or not. The value '1' is assigned to a pixel above the threshold and '0' to a pixel below this. To remove patches the image is further filtered.

(c) *Contour extraction and thinning*: For contour extraction the image is thinned by successive deletion of the outer layer of the image until a connected unit width framework or skeleton remains.

(d) *Modified optic flow algorithm*: The major modification in the algorithm proposed by Horn and Schunck are (i) *Symmetrisizing the algorithm*: This is achieved by computing 'backward looking' and 'forward looking' and matching, and averaging them together. By taking the middle as the reference frame an accurate value of the velocity is obtained. (ii) *Motion segmentation and matching region decision*: These are as suggested by Schunck[17] and are implemented as: The segmentation is performed by considering the flow direction and the axis of flow which is obtained from a contour of the image, if a shift in axis greater than 10° is obtained. Three frames are segmented and stored. For matching region decision, the motion of the pixel with its neighbours, a matching region in a 3×3 pixel is chosen. The matching strength (MS) obtained in frame '0' for a particular pixel is then searched in the next successive frames (frame '–1' and frame '1'). When a close match is obtained, the pixel is searched in the 3×3 region around it. This reduces the matching region to 3×3 pixels but in turn adds the calculation of MS of each pixel in two frames (forward and backward).

(e) *Algorithm*: The equation of motion using the above algorithm is given as

$$E_x + E_y + E_t = 0,$$

where E_x, E_y and E_t are partial derivatives along the x, y and t directions. The equation has two unknowns and cannot be used to calculate the axial and radial components U and V independently. An image smoothness constraint is introduced and the differential equations are solved by Gauss-Seidal method[18]. The solution is given below:

$$U^{n+1} = \bar{U}^n - E_x [E_x \bar{U}^n + E_y \bar{V}^n + E_t]/(\alpha^2 + E_x^2 + E_y^2),$$

$$V^{n+1} = \bar{V}^n - E_y [E_x \bar{U}^n + E_y \bar{V}^n + E_t]/(\alpha^2 + E_x^2 + E_y^2),$$

where $(\bar{U})$ and $(\bar{V})$ are the average velocities, n is the iteration index and α is the error weighing factor.

The calculation of $\bar{U}$, $\bar{V}$, E_x, E_y and E_t for a pixel is performed in a 3×3 region around (i, j) and an average

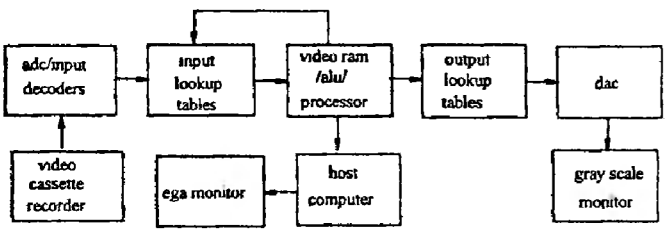

Figure 2. Schematic of the data analysis system.

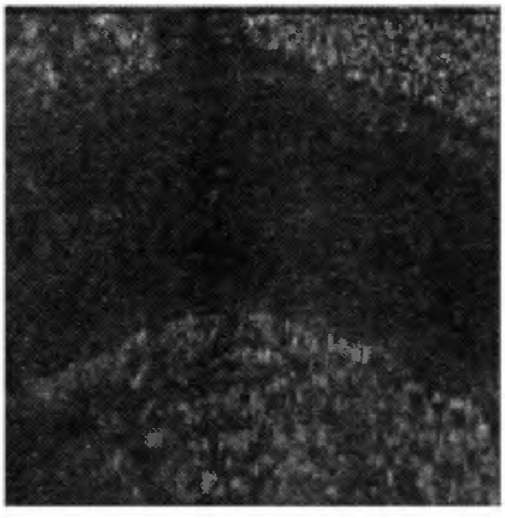

Figure 3. Microphotograph of the frog mesenteric branching artery.

value is used in the next iteration. This procedure is repeated until the error between the new estimated value and previous value of U and V is less than 0.001. The iterations are also stopped if no significant change in the new estimate is observed. The details of this procedure are given elsewhere[12]. Prior to measurement of the velocity by this procedure, the system was calibrated with a synthetic image displayed on the screen. By giving known displacement to this image in two successive frames the displacement values were calculated by image velocimetry. A highly significant correlation of measured and calculated values was obtained[12].

To determine the blood flow velocity the system was calibrated by a hemocytometer (Fein-Optik, Germany) with horizontal and vertical rulings of known dimensions. This was placed on the microscope stage and its image was obtained at the same magnification used for recording of blood flow. From the digitized image, the number of pixels occupied by the grid of area 1 mm^2 was determined. Based on this the calculated length of one pixel was 0.78125 μm. Using this length, the displacement of blood cells between successive frames was determined. Dividing this by the video frame rate the blood flow was determined.

Flow cycle is determined by the variation of the flow velocity over a sequence of images and that represents a cardiac cycle. This is important for fixing a reference point for further analysis of data. For this purpose 64 sequential frames are analysed by the velocimetry algorithm to obtain the displacements in all the frames at the center of the upstream section of the main artery located perpendicular to the vessel wall. Three successive processed frames 1, 2 and 3 are used and the vector velocity is determined. By a similar procedure all successive frames are analysed. The displacements at these locations are plotted at their respective velocities. The interval between two successive maxima corresponds to the cardiac cycle. Since both the U and V components which vary in the curved section of the artery contribute to the flow velocity, the axial velocity was further matched for exact determination of the cardiac cycle.

The contour of the vessel wall in the image is detected by edge detection, thresholding and thinning operations. From this, the axis is determined, which is parallel to the vessel walls. Thereafter, the edge detected and thresholded image is scanned along all the columns perpendicular to the axis. The number of pixels between the first '1' and the last '1' is equal to the thickness of upper wall of the vessel. Scanning is continued along the same vertical column until the next '1' is detected. Number of pixels between this detected '1' and the previous '1' is equal to the inner diameter of the artery. Scanning is further continued and when '1' is detected the number of pixels up to the last '1' are counted. This gives the thickness of the lower wall of the vessel and the average mean thickness of the vessel wall (in pixels) and was converted into μm by multiplying with the pixel value in μm.

From the axial and radial velocity components, the magnitude of the vector velocity is calculated, from whose value at all locations along the diameter the

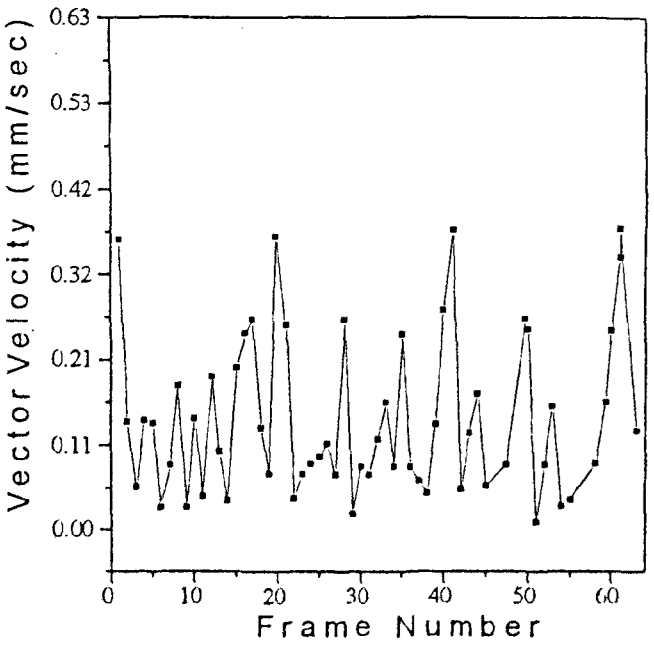

Figure 4. Variation of calculated vector velocity at the axis of the artery over 64 frames.

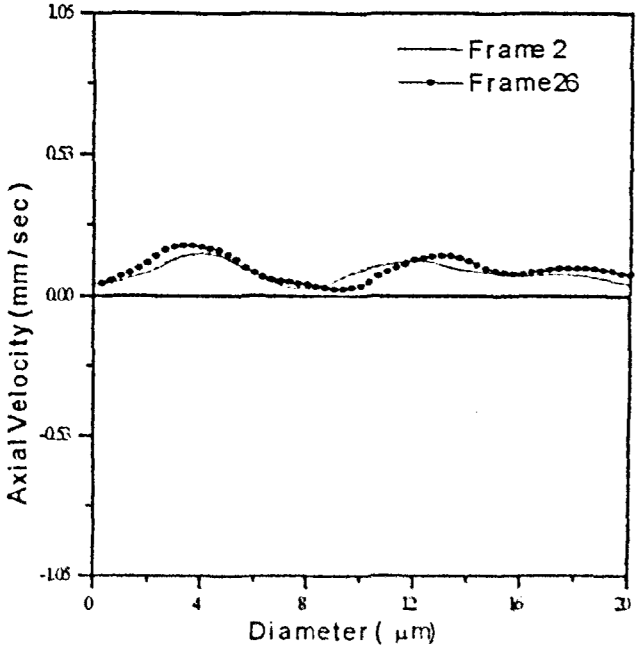

Figure 5. Comparison of the maximum axial velocity during frames 2 and 26 corresponding to a flow cycle.

mean velocity is calculated by

$$U_{mean} = \frac{\Sigma x_i w_i}{\Sigma x_i}.$$

where x_i = position along the diameter, w_i = flow velocity at x_i given by $\sqrt{u_i^2 + v_i^2}$.

Figure 3 shows the microphotograph of the frog mesenteric artery. The wall thickness of the main artery is 4 μm. The radii of the main and branch arteries are 20 μm and 6 μm. The ratio of the radius of the artery to radius of curvature is 0.156. Figure 4 shows the velocity variation over 64 frames. According to this the spacing between the velocity maximum varies from 20 to 21 frames. As this velocity is contributed by U and V, the cardiac cycle is further confirmed by comparison of axial velocity. For this purpose the axial velocity at the same location is calculated from 1 to 30 frames. Its variation along the diameter obtained at frame 2 is compared with that as observed at other frames. Figure 5 shows the matching of this velocity component at frames 2 and 26. The maximum and minimum of this component occur at frames 2 and 24. The data in these frames are used for further analysis.

Figure 6 shows the processed contour of the branching artery and the various locations in the main artery. The positions 1–4 and 6–9 hereafter will be referred to as the upstream and downstream locations of the main artery, respectively. The angles subtended with the horizontal of various sections are also given. Due to the short length of the branch available only one location is chosen for analysis. For sequential analysis of pulsatile flow cycle, four locations are chosen and they are at frames 2, 7, 14 and 24.

Figure 7 *a–d* show the variation of axial velocity at various locations in the arteries. The axial velocity is maximum in the branch artery (Figure 7 *a*). A varying pattern of velocity in the upstream and downstream sections is observed. The velocity in the branch artery is the maximum in the forward direction. A shift in this component towards the lower wall is observed. Figure 7 *b* shows the variation of the axial velocity at frame 7. The upstream axial velocity is reduced, whereas downstream components show an increasing trend. The magnitude of the velocity in the branch is reduced. With the progression of the cardiac cycle, the magnitude of this is further reduced and after minimum this reverses to negative.

Figure 7 *c* shows a negative shift of this component at frame 14. At this stage a shifting trend in the upstream and downstream axial velocity is observed. An increased value of axial velocity at the lower wall shift towards the centre. The transition of velocities at flow reversal in the branch takes place at frame 24 (Figure 7 *d*). The magnitude of the axial velocity in the upstream branch is also reversed being maximum at the location near the branch but downstream a varying trend is observed. This could be attributed to flow reversal in the branch artery which attains a value similar to that as during systolic phase.

Table 1 shows the variation of the mean velocity at various locations in the main and branch arteries. Due to the small diameter of the branch artery the mean velocity in this vessel is significantly higher than that in the main artery. The effect of flow reversal on the mean velocities in the main artery is clearly shown. Based on the values of the mean velocity various flow related parameters are calculated. The values of Reynold's number and the Womersley parameter for the main

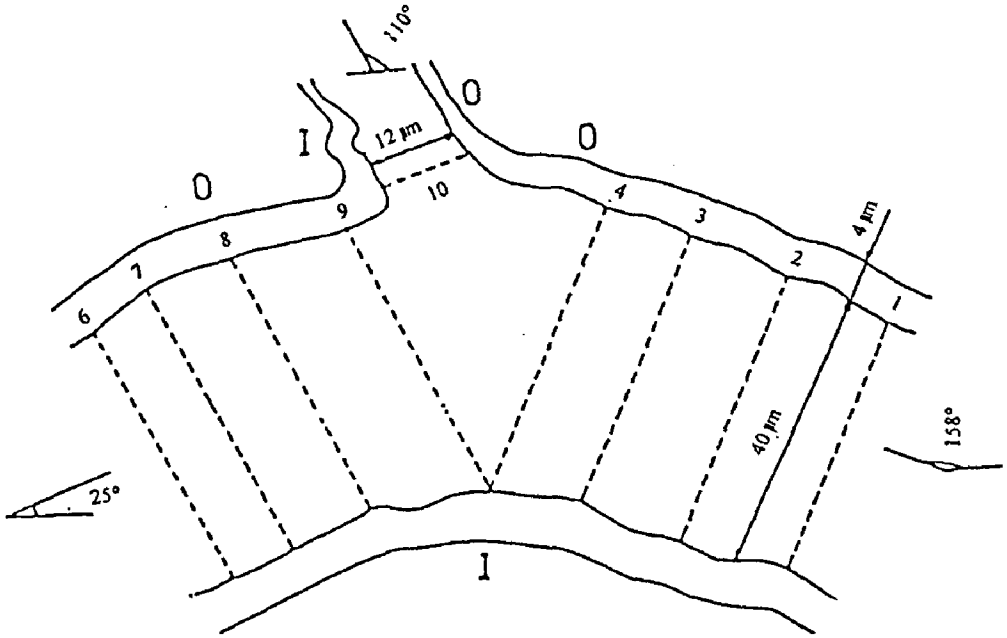

Figure 6. Contour of the main and branching arteries with various locations for velocity calculations.

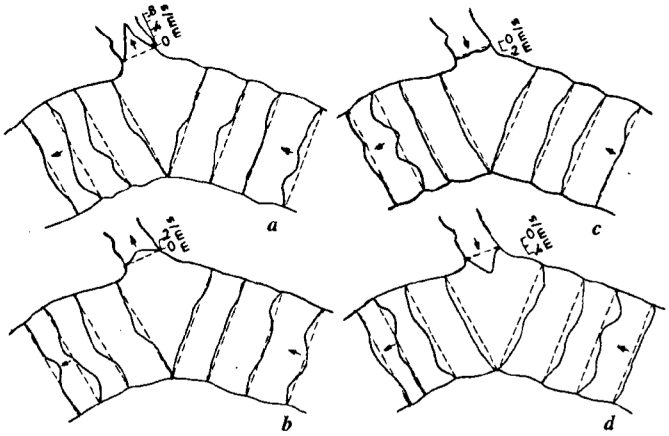

Figure 7 *a–d*. Axial velocity variation at various locations in frames 2, 7, 14 and 24 during various phases of the cardiac cycle. The blood flow through branch artery which reverses during diastolic phase is also shown.

artery obtained during systolic phase are 0.457 and 0.248, respectively. The Dean's number for the same artery is 0.359.

The present technique is based on on-line recording and off-line processing of data. The video-microscopic images consist of noise contributed by several factors including optical scattering from flowing erythrocytes, optical noise from video cameras and recording and reproduction of the video cassette recorder. Hence the images are pre-processed prior to calculation of velocity data.

Blood flow through the curved tube has been simulated experimentally and theoretically. The peak axial velocity vacillates across the horizontal diameter, which is in agreement with that reported by others[19]. In the upstream region the maximum axial velocity occurred nearest to the outer wall. During forward flow we have also found a similar peak after 200 msec of the occurrence of the maximum. The radial velocity component dominates the lower region on the artery indicating the presence of secondary flow in these regions, which supports the theoretical findings of others[20]. As stated earlier, these models in the absence of branching arteries do not correspond to the actual aortic flow. For this purpose a further comparison is carried out with the work reported by Leipsch *et al.*[21]. The velocity at the branching is found to be higher than that of the main vessel which is similar to our observations.

During flow reversal under minimum flow conditions in the branch a pattern similar to that of forward flow is repeated in the branch artery. This affects the flow in the upstream portion of the main artery which shows a reversal of axial velocity in the upstream part, whereas in the downstream part a distinct pattern of flow with positive axial mean velocity is maintained. Thus the flow through the branch affects the flow through the main artery. In addition to this the maximum of the axial velocity is affected by the length of the artery and the branch location[1].

Table 1. Mean velocity at various locations at frames 2 and 24

Position	Mean velocity (mm/sec)	
	Frame 2	Frame 24
1	0.096	0.172
2	0.067	0.230
3	0.098	0.287
4	0.090	0.219
5	0.097	0.227
6	0.071	0.222
7	0.024	0.334
8	0.007	0.293
9	1.090	0.942

In conclusion, this technique could successfully be used not only to determine the velocity profiles in and around complex geometries but also for measurement of vessel thickness and its diameter. It could be used on any location where a sequence of images is recorded and also provide flexibility to choose any location for calculation of these parameters.

1. Liepsch, D., *Biorheology*, 1986, **23**, 395.
2. Pedley, T. J., *The Fluid Mechanics of Large Vessels*, Cambridge Univ. Press, Cambridge, 1980, pp. 161–171.
3. Petrig, B. L. and Riva, C. E., *Appl. Opt.*, 1985, **27**, 1126.
4. Wayland, H. and Johnson, P. C., *J. Appl. Physiol.*, 1967, **22**, 333.
5. Sato, M. and Ohshima, N., *Biorheology*, 1988, **25**, 279.
6. Seki, J. and Lipowski, H. H., *Microvas. Res.*, 1989, **38**, 110.
7. Hesselink, L., *Ann. Rev. Fluid Mech.*, 1988, **20**, 421.
8. Prakash, B. and Singh, M., *J. Biomech.*, 1995, **28**, 649.
9. Prakash, B. and Singh, M., *Biorheology*, 1996, **33**, 59.
10. Kak, A. C., *Proc. IEEE*, 1979, **67**, 1345.
11. Horn, B. K. and Schunck, B. G., *Art. Intell.*, 1981, **17**, 185.
12. Umrani, J., Prakash, B. and Singh, M., *Med. Biol. Eng. Comput.*, 1997, **35**, 373.
13. Agarwal, J. K. and Nandakumar, N., *Proc. IEEE*, 1988, **76**, 917.
14. Douglas, M. A. and Trus, B. L., *Med. Prog. Technol.*, 1989, **15**, 109.
15. Rosenfeld, A. and Kak, A. C., *Digital Picture Processing*, Academic Press, 1982.
16. Smith, R. W., *Computer Processing of Line Images: A Survey. Pattern Recognition*, 1987, **20**, 7.
17. Schunck, B. G., *Proc. Workshop on Computer Vision*, Annapolis, 1991, pp. 58–62.
18. Scarborough, J. B., *Numerical Mathematical Analysis*, Oxford and IBH Publications, 1966.
19. Chandran, K. B. and Yearwood, T. L., *J. Fluid Mech.*, 1981, **111**, 59.
20. Chang, L. J. and Tarbell, J. M., *J. Fluid Mech.*, 1985, **116**, 175.
21. Liepsch, D., Moravec, S. T. and Baumgart, R., 1992, **29**, 563.

Received 12 June 1998; revised accepted 22 July 1998.